

Contents lists available at ScienceDirect

Analytica Chimica Acta

journal homepage: www.elsevier.com/locate/aca



Infrared laser ablation sampling coupled with data independent high resolution UPLC-IM-MS/MS for tissue analysis



Michael E. Pettit ^a, Fabrizio Donnarumma ^b, Kermit K. Murray ^b, Touradj Solouki ^{a, *}

- ^a Department of Chemistry and Biochemistry, Baylor University, Waco, TX, 76798, USA
- ^b Department of Chemistry, Louisiana State University, Baton Rouge, LA, 70803, USA

HIGHLIGHTS

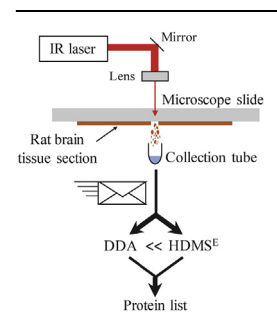
- IM/MS analyses of laser ablated tissue samples provide improved proteomics characterization.
- LC, IM, and MS provide analyte specific three-dimensional addresses in an increased data volume.
- Data independent high definition MS (HDMS^E) proteomics work flows can reduce analysis time.
- Combined use of data dependent analysis (DDA) and HDMS^E yields improved protein identification.

ARTICLE INFO

Article history:
Received 5 April 2018
Received in revised form
22 June 2018
Accepted 24 June 2018
Available online 26 June 2018

Keywords:
Mass spectrometry
Proteomics
Data-dependent acquisition
IM-Enhanced data-independent acquisition
IR laser ablation

G R A P H I C A L A B S T R A C T



ABSTRACT

Infrared laser ablation microsampling was used with data-dependent acquisition (DDA) and ion mobility-enhanced data-independent acquisition (HDMS^E) for mass spectrometry based bottom-up proteomics analysis of rat brain tissue. Results from HDMS^E and DDA analyses of the 12 laser ablation sampled tissue sections showed that HDMS^E consistently identified approximately seven times more peptides and four times more proteins than DDA. To evaluate the impact of ultra-performance liquid chromatography (UPLC) peak congestion on HDMS^E and DDA analysis, whole tissue digests from rat brain were analyzed at six different UPLC separation times. Analogous to results from laser ablated samples, HDMS^E analyses of whole tissue digests yielded about four times more proteins identified than DDA for all six UPLC separation times.

© 2018 Elsevier B.V. All rights reserved.

1. Introduction

High-throughput identification and quantification of the constituent biomolecules in tissue is a significant challenge for biological mass spectrometry [1]. Compound identification is particularly difficult in conventional mass spectrometry imaging

because tissue sampling and ion introduction to the mass spectrometer are typically performed concurrently, precluding many advantageous processing and separation steps. Quantification of material directly ionized from tissue is challenging because the desorption and ionization processes are sensitive to sample morphology [2] and to signal suppression from components in the complex mixtures of compounds [3,4]. In the case of MALDI imaging, there is the additional challenge of homogeneous matrix addition [5].

Identification and quantification of compounds in tissue can be improved by sample extraction and subsequent off-line mass

^{*} Corresponding author. Department of Chemistry and Biochemistry, Baylor University Sciences Building, One Bear Place #97348, Waco, TX, 76798, USA. E-mail address: Touradj_Solouki@baylor.edu (T. Solouki).

spectrometry analyses [6–10]. Extraction of material from tissue for off-line LC-MS and MS/MS analysis can be done with complete sections [11-13], excised portions of tissue [6,7,14], or by localized sampling [12]. Tissue sections can be manually dissected, for example, using a thin plastic film to assist in region of interest (ROI) selection for compound extraction [6,15,16]. In this technique, MALDI mass spectrometry is used to identify regions of interest (ROIs): consecutive sections are subsequently deposited on parafilm covered glass microscope slides and ROIs are manually excised. Laser microdissection uses a laser in conjunction with an optical microscope to select portions of a tissue section for removal [17-19]. Laser microdissection systems use either an ultraviolet (UV) laser to cut the tissue or an infrared laser to melt a plastic film to physically capture the tissue. Microdissected regions can be analyzed directly using mass spectrometry [20–23] or with liquid chromatography coupled with mass spectrometry [24–28].

We have developed an infrared laser ablation microsampling method [32-34] that has advantages of speed and efficiency compared to laser microdissection, ablation at UV laser wavelengths [29], and surface sampling [30—31]. Using an IR laser, tissue is ablated and captured in a solvent therefore this sampling method does not require coated slides or thermal polymer and does not require cell lysis by sonication or the addition of detergent. Unlike a liquid microjunction, laser ablation removal does not require surface contact which can reduce analyte diffusion and memory effects. We have coupled laser ablation sampling to liquid chromatography and tandem mass spectrometry for proteomic analysis of tissue [35].

Tandem mass spectrometry has traditionally been performed using DDA, where the most abundant precursor ions are selected one at a time for fragmentation [36]. Data independent acquisition (DIA) is a more recent approach that applies fragmentation to all ions within a large m/z range [37–45]. With DIA, an entire m/z range of interest is probed by precursor ion scans (MS1) followed by product ion scans (MS2) in which all detectable ions are fragmented within either sequentially scanned smaller windows (ranging from ~2.5 Da to ~20 Da) [37,38,40-42,45] or the full m/zrange [39,43,44]. Fragmentation of all ions in a large m/z range can lead to higher dynamic range, better sensitivity, and better quantification accuracy [24]. The use of alternating low and high collision-energy in DIA facilitates multiplex detection of precursor and product ions (analogous to Fellgett's advantage [46]) and can result in a near 100% duty cycle [24]. Currently, "all ion fragmentation" strategies are licensed by Thermo Scientific as "DIA", AB Sciex as "sequential window acquisition of all theoretical spectra" (SWATH), Agilent as "All Ions MS/MS", and Waters as "MS^E". During LC-MS^E experiments, the full m/z range is probed using continuously alternating MS1 and MS2 scans. Ion mobility (IM) [47-50] with LC-MS^E [51] is a recent approach to DIA called HDMS^E. Data acquisition for HDMS^E is in three-dimensions: LC retention time, IM drift time, and m/z. Specifically, in HDMS^E, IM drift time and accurate mass and retention time (AMRT) correlation are used to facilitate assignment of precursor and product ions from the threedimensional data [52-55].

In this work, we report on the use of DDA and HDMS^E for analysis of laser ablated tissue samples. Here, we use laser ablation sample transfer (LAST) for biomolecule extraction from rat brain tissue sections to compare bottom-up protein identification by DDA and HDMS^E acquisition. Using whole tissue digests from rat brain, we also examine the effect of UPLC separation time on the number of peptides and proteins identified by DDA and HDMS^E.

2. Materials and methods

Laser ablation sample transfer and trypsin digestions were performed at Louisiana State University (LSU), and all MS experiments and data processing were carried out at Baylor University (BU).

2.1. Chemicals, supplies, and solvents

Trimethamine (tris) base was purchased from Bio-Rad (Hercules, CA, USA). DL-dithiothreitol (DTT, 98%), iodoacetamide (IAA, BioUltra, 99%) and ammonium bicarbonate (ABC, BioUltra, 99.5%) were obtained from Sigma-Aldrich (St. Louis, MO, USA). Tris (50 mM) and ABC (10 mM) buffers were adjusted to pH values of 8.5 and 7.4, respectively. Sequencing grade modified trypsin was purchased from Promega (Madison, WI, USA).

Ultrapure water with an overall ionic concentration of <0.1 ppb and resistivity of ~18.2 M Ω cm at 25 °C was produced in-house, using either a NANOpure ultrapure water system at LSU (Barnstead, Van Nuys, CA, USA) or a Direct-Q 3 UV water purification system at BU (EMD Millipore Corporation, Billerica, MA, USA). Ultracentrifugation cartridges (10 kDa cutoff) were obtained from Pall (Port Washington, NY, USA). Glass microscope slides (25 × 75 mm) were obtained from VWR (West Chester, PA, USA). Sodium formate and [Glu¹]-fibrinopeptide B were purchased from Waters Corp. (Milford, MA, USA). Acetic acid, acetonitrile (ACN, \geq 99.9%), formic acid (FA), and methanol (\geq 99.9%) were purchased from Fisher-Scientific (Waltham, MA, USA).

2.2. Tissue samples

Tissue samples were obtained from four-week-old breeding rats at the Louisiana State University School of Veterinary Medicine Division of Laboratory Animal Medicine (DLAM). All protocols for animal care and use were approved by the Institutional Animal Care and Use Committee at LSU, and samples were handled as outlined by the Department of Environmental Health and Safety at BU. The animals were sacrificed by CO_2 (5 psi) exposure. Brain samples were collected, washed in 50 mM ammonium bicarbonate buffer for 30 s, and frozen in liquid nitrogen within 30 min. Frozen samples were stored at $-80\,^{\circ}$ C. Thin sections were prepared with a Leica CM1850 cryostat (Leica Microsystems, Wetzlar, Germany) directly from the frozen tissue. Optimal cutting temperature (OCT) solution was used to fix one side of the sample to the cryostat support. Coronal rat brain sections were cut at a thickness of 50 µm, thaw-mounted on uncoated microscope slides, and stored at $-80\,^{\circ}$ C.

2.3. Laser ablation sample transfer

Tissue sections were dried under vacuum for 30 min prior to sampling. Laser ablation and material collection were performed as previously described [35]. Ablation was conducted on 2×2 mm regions at a laser fluence of 27 kJ m $^{-2}$ using an OPO IR laser (IR Opolette, OPOTEK, Carlsbad, CA, USA) at 2940 nm wavelength. After ablation, the microcentrifuge tubes containing the captured sample (collected in liquid) [35] were vortexed for 30 s and stored at $-20\,^{\circ}$ C until filter aided sample processing.

2.4. Microscopy imaging

Microscopy images were acquired with a fluorescence stereomicroscope (SteREO Lumar V12, Zeiss) equipped with a $0.8 \times \text{Neolumar}$ S objective and a high resolution digital camera (AxioCam HRc, Zeiss). Images were recorded in bright field mode and exported using Zen 2012 software (Zeiss).

2.5. Filter aided sample processing

Proteomic sample processing was performed at LSU as

previously described [35]. Whole tissue samples were collected in tubes, and after addition of 500 µL of tris buffer (50 mM, pH 8.5), they were homogenized with a high-power ultrasonic homogenizer (Sonifier S-450, Emerson Electric, St. Louis, MO); LAST samples were not subjected to ultrasonic homogenization. Protein disulfide bond reduction was achieved by adding DTT to each tube to a final concentration of 10 mM. Samples were incubated at 80 °C for 45 min, and after cooling at room temperature for 15 min. transferred to ultrafiltration cartridges with a molecular weight cutoff of 10 kDa and centrifuged at 14,000 g for 20 min. Alkylation was performed by adding 100 µL of a 20 mM IAA solution to each unit followed by incubation in the dark for 30 min. After incubation, the samples were centrifuged again at 14,000 g for 10 min. Buffer exchanges and washing steps were performed by adding 100 µL of ABC buffer to each tube and centrifugation at 14,000 g for 10 min. This step was repeated twice, after which filter units were placed in clean tubes. Enzymatic digestion of the protein material was achieved using 50 μ L of ABC buffer and 1 μ L of a 50 ng μ L⁻¹ trypsin solution. Samples were incubated at 37 °C overnight and shaken at 200 rpm. After digestion, the filter units were centrifuged at $14,000 \, g$ for $10 \, min$, $50 \, \mu L$ of ABC buffer were added, and filter units were centrifuged again. No additional desalting step (e.g., C18 tips) was used after filter aided sample processing. The filter units were removed and the tryptic mixtures were vacuum dried. The centrifuge tubes containing the dried samples were packaged in dry ice and shipped to Baylor where they were stored at -40 °C before use.

Prior to MS analyses, dried samples were thawed and resuspended in aqueous solutions containing 5% ACN and 0.1% FA. Based on a previous protocol [35], sample concentrations were ~80 ng μL^{-1} and ~184 ng μL^{-1} for the digested LAST and whole tissue samples, respectively. The re-suspended samples were vortexed for 30 s using a vortex mixer (VWR International, Radnor, PA) and centrifuged at 1000 g for 1 min using a microcentrifuge (Sorvall Legend Micro 21R, Thermo Scientific, Waltham, MA); the vortex/centrifuge step was repeated once.

2.6. UPLC-MS/MS

The ultra-performance LC-MS/MS (UPLC-MS/MS) method was adapted from Geromanos et al. [24]. Separation of tryptic peptides was performed using a UPLC system (nanoAcquity, Waters Corporation, Milford, MA) equipped with a Symmetry C18 pre-column (5 μm , 20 mm \times 180 μm) and a BEH130C18 analytical reversedphase column (1.7 μ m, 100 mm \times 100 μ m). Mobile phase solvents A and B were water and ACN, respectively (each with 0.1% FA). For each sample, a $4.0\,\mu L$ partial loop injection was transferred to the pre-column for desalting and pre-concentration using 99% solvent A at a flow rate of $10 \,\mu L \, min^{-1}$ for 3 min. The pre-concentrated peptides were eluted to the analytical column and separated using a gradient of 5%–45% solvent B at a flow rate of 600 nL min⁻¹; a 90-min separation was performed unless otherwise stated. Following separation, the mobile phase was ramped to 99% solvent B for 5 min and held at 99% solvent B for an additional 5-min. The mobile phase was ramped to 5% solvent B over 5 min, and the column was re-equilibrated at 5% solvent B for 15 min. Throughout the separation, the UPLC column temperature was held at 40 °C. The lock mass compound, [Glu¹]-fibrinopeptide B at a concentration of 300 fmoL μ L⁻¹, was delivered at 500 nL min⁻¹ by the auxiliary pump of the UPLC system to the reference sprayer of the NanoLockSpray source of the mass spectrometer. To minimize disparities, DDA and HDMS^E runs were made in alternating order.

MS was performed in positive-ion electrospray ionization (ESI) mode using a Synapt G2-S HDMS (Waters, Milford, MA) that was set to sensitivity mode (V mode), with a typical mass resolving power $(M/\Delta M_{50\%})$ of ~10,000. The time-of-flight (TOF) analyzer was

externally calibrated with a sodium formate solution from m/z 50 to 2000; all samples were measured in the same m/z range of 50 to 2000. The reference sprayer was sampled every 30 s, and all TOF MS data were lock mass corrected (post acquisition) using the doubly-charged monoisotopic ions of [Glu¹]-fibrinopeptide B at m/z 785.8426. The IM drift cell was filled with nitrogen gas during HDMS^E experiments at direct measurement readout of ~3.5 mbar N₂.

UPLC data-dependent acquisition (UPLC-DDA) was accomplished using the "Fast DDA" function of MassLynx (Ver. 4.1, Waters: Milford, MA) as follows: MS survey scans were acquired for all detectable ions using a 4V transfer collision-energy for 0.6 s, precursor ions in the MS survey scans that were measured as 2^+ , 3^+ or 4⁺ charged ions were selected for MS/MS, and MS/MS data were obtained for up to three precursor ions detected in each survey scan. Please note that charge-state restrictions were utilized during DDA to increase the number of tryptic peptide precursor ions selected for MS/MS. For each precursor ion selected from the survey scan, MS/MS data were collected at a scan time of 0.3 s, using a transfer collision-energy ramp from 15 V to 45 V. A dynamic exclusion window of 0.100 Da was set to 60 s to avoid unnecessary repetition of MS/MS for observed common ions within the 60 s window periods. Acquisition automatically switched from MS to MS/MS mode when the base peak intensity exceeded a threshold of 150 counts s^{-1} and returned to MS mode after a maximum of three MS/MS scans were acquired per selected ion (i.e., maximum of 0.9 s for one ion): the mass spectrometer also switched from MS/MS mode to MS mode when the TIC in the MS/MS function exceeded 8.000.000 counts s⁻¹. A 0.01 s inter-scan delay was used and thus each MS scan and associated MS/MS scans required a minimum of 1.54 s and a maximum of 3.4 s.

UPLC data-independent acquisition (UPLC-HDMS^E) was accomplished using the IM-enhanced "MS^E Continuum" function of MassLynx which utilizes IM separation in conjunction with TOF detection, using alternating low and high collision-energies. The acquisition times for the low and high collision-energy scans were 1 s each. The low energy scans were collected using a constant 4 V transfer collision-energy. For the high-energy scans, the transfer collision-energy was ramped from 15 V to 45 V during each 1 s data integration. A 0.015 s inter-scan delay was used and thus a pair of low and high collision-energy scans was collected every 2.030 s. Although all experimental parameters for HDMS^E and DDA were not identical, both approaches were independently optimized for realistic comparisons of data.

2.7. Data analysis

Peptide detection from raw DDA and HDMS^E datasets was accomplished with ProteinLynx Global Server (PLGS Ver. 2.5.2; Waters Corporation, Milford, MA) using the default processing parameters specific to "Electrospray DDA" and "Electrospray MS^E" in PLGS data modes, respectively. Because precursor ion selection (i.e., m/z isolation in the quadrupole) is utilized in DDA prior to collecting MS/MS data, product ions are readily assigned to their respective precursor ions via PLGS data processing; HDMS^E does not utilize precursor ion selection, therefore, product ions are correlated to their corresponding precursor ions by PLGS via LC retention time and IM drift time alignments. Once precursorproduct ion correlations have been generated by PLGS for DDA and HDMS^E datasets, the same algorithm is used for peptide detection. Peptides identified by PLGS with sequence lengths greater than 5 amino acids were utilized for a customized BLAST search against a UniprotKB/Swiss-Prot database [56] that contained 9676 protein entries (8126 proteins and 1641 isoforms) corresponding to the Rattus norvegicus proteome (version 2017_11,

accessed December 18, 2017). Database searching BLAST command line tool (PeptideMatchCMD version 1.0) from the Protein Information Resource (PIR) [57] was used. The resulting protein matches were filtered to retain only proteins with at least two matched peptides and database search results were manually compared using a spreadsheet. All averaged values are reported as 95% confidence intervals with n=12.

3. Results

Rat brain tissue extracts were obtained from 2×2 mm regions of tissue sections via LAST for DDA and HDMS^E analysis. Whole tissue digests were obtained from the same rat specimen and used to examine the impact of separation time on DDA and HDMS^E protein identification. The collected material was subjected to enzymatic digestion prior to bottom-up proteomics analysis. Duplicate UPLC-DDA and duplicate UPLC-HDMS^E experiments were performed on laser ablated samples such that each sample obtained via LAST was measured a total of four times. Six UPLC-DDA and six UPLC-HDMS^E experiments, corresponding to separation times of 15, 30, 60, 90, 120, and 150 min, were performed on aliquots of a whole tissue digest sample. Raw UPLC-DDA and UPLC-HDMS^E data were processed and searched as indicated above.

3.1. DDA and HDMS^E of brain tissue extracts collected via LAST

Fig. 1 shows an optical microscopy image of a coronal rat brain tissue section (Section 1) after sample collection via LAST. Each of the four laser-ablated (2×2 mm) regions correspond to a tissue sampling quadrant and are labeled Q1, Q2, Q3, and Q4. The tissue sections were 50 μ m thick, and an estimated ~2 μ g of material was removed from each quadrant [35]. Three consecutive tissue sections from the same animal were used to obtain the MS results from the twelve sampled positions. The samples are identified by quadrant and section; for example, the sample obtained from Quadrant 1, Section 1 is identified as Q1S1, and so on. Microscopy images of S2 and S3 before and after LAST are shown in Supporting Figure S-1. Please note that equivalent quadrants extracted from consecutive sections (e.g., Q1S1, Q1S2, and Q1S3) should not be considered technical replicates because they do not correspond to the same physical x-, y-, and z-coordinates of the brain.

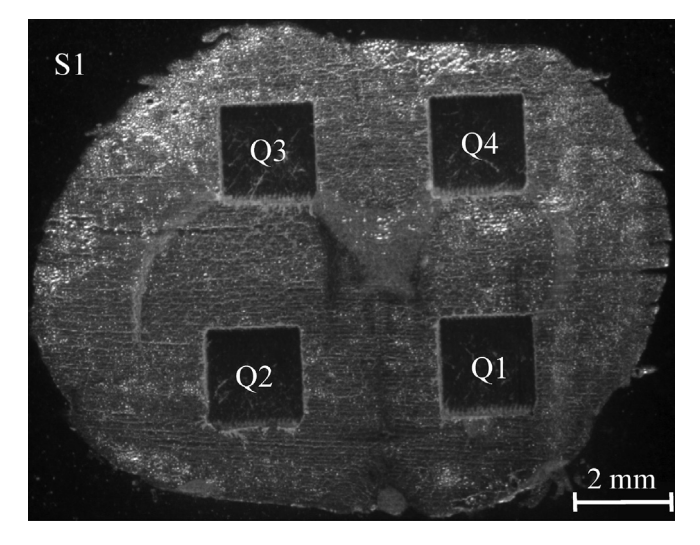


Fig. 1. Microscopy image of rat brain whole tissue section 1 (S1) after tissue extraction *via* LAST. Rat brain tissue was collected from four spatially localized quadrants of the brain. Sampling quadrants 1 through 4 are indicated by Q1, Q2, Q3, and Q4.

Fig. 2 shows representative base peak chromatograms (BPCs) and examples of extracted mass spectra (XMS) generated from UPLC-DDA and UPLC-HDMS^E acquisitions of Q1S3. Representative BPCs from DDA (Fig. 2a) and HDMS^E (Fig. 2b) correspond to peptide elution. Corresponding precursor ion XMS for the indicated retention times are shown in Fig. 2c through 2f. The precursor ion data was extracted from MS survey scans collected at a collisionenergy of 4V. This energy was selected to minimize unwanted peptide fragmentation for collection of MS survey scans during both DDA and HDMS^E [58]. The chromatography data span the retention time interval from 0 to 65 min corresponding to the gradient of 5%-~34% solvent B. Chromatographic features in representative BPCs from DDA and HDMS^E runs are within ~2.5 s of each other. The small LC retention time (t_R) difference for replicate trials is not excessive [59,60] and could be caused by differences in mobile phase pH [61] from solvent evaporation or ingress of CO₂.

Representative precursor ion mass spectra generated from DDA and HDMS^E are shown in Fig. 2c through 2f and correspond to peptides eluting at 11.4, 29.6, 42.1, and 52.2 min, respectively. Comparison of mass spectra in Fig. 2c through 2f shows that DDA (left) and HDMS^E (right) generate similar precursor ion mass spectra and this confirms the chromatographic alignment between the two data sets. For example, in both DDA and HDMS^E, the peptide AGFAGDDAPR eluted at $t_R = 11.4 \text{ min}$ (Fig. 2c). Fig. 2d shows the mass spectra for LLIEMEQR peptide at $t_R = 29.6 \text{ min}$ for UPLC-DDA and UPLC-HDMS^E. Similarly, chromatographic peaks at $t_R = 42.1 \text{ min for AILVDLEPGTMDSVR (Fig. 2e)}$ and at $t_R = 52.2 \text{ min}$ for LICCDILDVLDK (Fig. 2f) were observed. The reported m/z values (i.e., 488.72, 516.29, 808.40, and 738.85) are from MassLynx output prior to PLGS processing and within 50 ppm of their respective theoretical masses. The peptide LICCDILDVLDK in Fig. 2f was detected in its modified form with carbamidomethylation of both cysteines. Corresponding MS/MS spectra for the peptides AGFAGDDAPR, LLIEMEQR, AILVDLEPGTMDSVR, and LICCDILDVLDK are shown in Supporting Figure S-2.

The MS peak intensity maxima in the precursor ion scans were generally lower for DDA than MS^E, presumably because of the lower MS signal averaging in DDA [24]. However, in comparison to MS^E (data not shown), the use of ion mobility in HDMS^E reduced ion transmission by an order of magnitude, which may be due to scattering collisions between analyte ions and IM drift gas [62,63]. This is reflected in greater intensities in the BPC of DDA compared to HDMS^E (Fig. 2a and b).

Results from UPLC-DDA and UPLC-HDMS^E analyses of the brain tissue samples collected via LAST are summarized in Table 1. For each of the twelve LAST samples (Column 1), the number of proteins identified by DDA (Column 2) or HDMS^E (Column 3), the total number of proteins (Column 4, excluding duplicate protein identification), proteins identified by DDA only (Column 6) or HDMS^E only (Column 7) are reported in Table 1. For all twelve sampling quadrants HDMS^E identified more proteins than DDA. This enhancement ranged from a factor of about two and a half (Q1S1, Table 1) to five and a half (Q3S1), and the averaged enhancement for all twelve quadrants was approximately a factor of four. Although HDMS^E provided more proteins for all twelve laser ablation samples, some proteins were identified by either DDA only or HDMS^E only (viz., Columns 6 and 7 in Table 1). On average, for all sampling quadrants, about 2% of the total proteins identified were found only by DDA analysis; about 73% of the total proteins identified were found only via HDMS^E (~25% were identified by both techniques).

Protein overlap, in terms of detection of proteins that were common to multiple sampling quadrants/sections, was expected due to the presence of highly concentrated, relatively ubiquitous proteins in tissue (*e.g.*, hemoglobin, albumin, actins, tubulins, *etc.*).

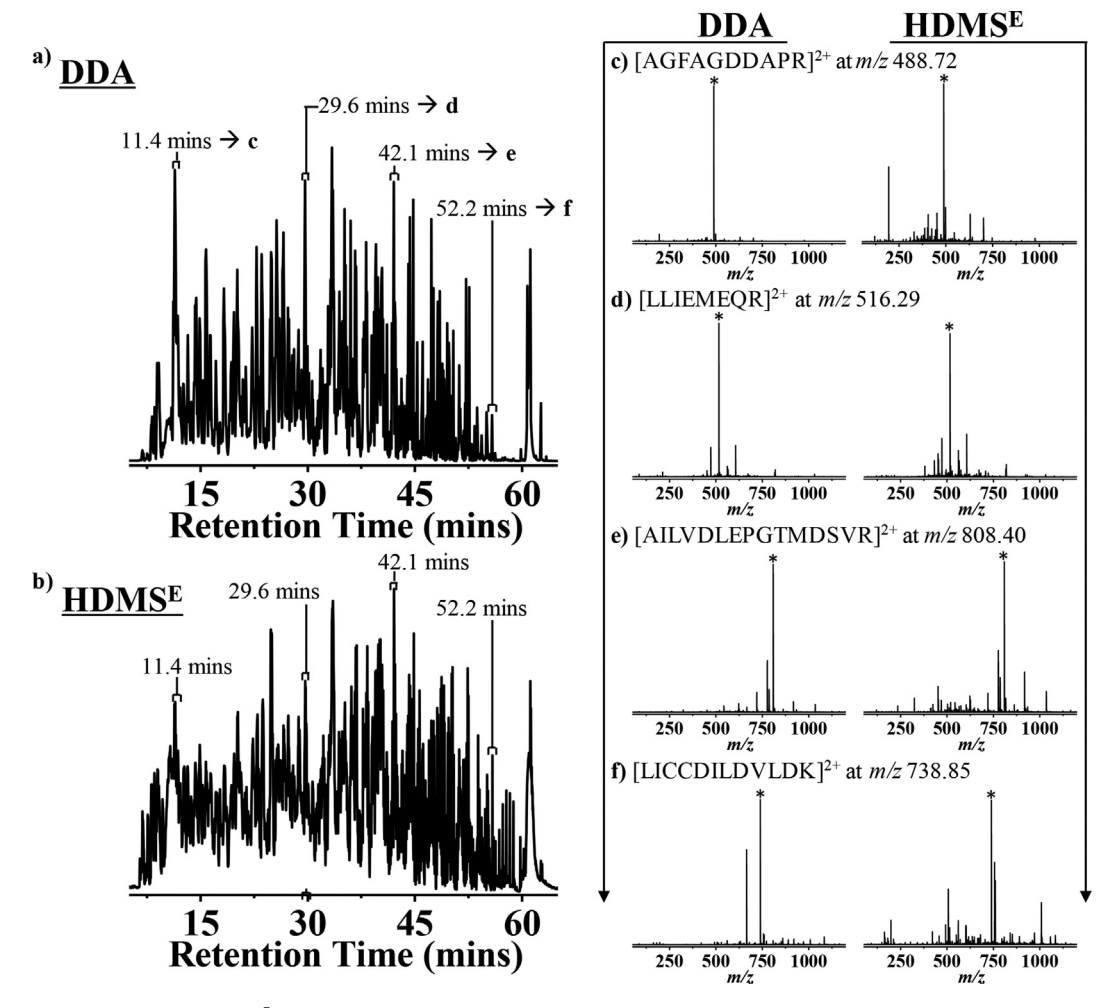


Fig. 2. Representative UPLC-DDA and UPLC-HDMS^E data from analyses of Q1S3. Base peak chromatograms (BPCs) corresponding to peptide elution from (a) DDA and (b) HDMS^E data acquisition modes. For peaks at 11.4, 29.6, 42.1, and 52.2 min, precursor ion mass spectra are in (c)—(f) for DDA (left) and HDMS^E (right). Precursor ion mass spectra of (c) [AGFAGDDAPR]²⁺ at m/z 488.72, (d) [LLIEMEQR]²⁺ at m/z 516.29, (e) [AILVDLEPGTMDSVR]²⁺ at m/z 808.40, and (f) [LICCDILDVLDK]²⁺ at m/z 738.85. The base peak in each mass spectra is designated with (*) and corresponds to the named precursor peptide ion.

Table 1Summary of proteins identified by DDA and HDMS^E analyses of the 12 laser ablation sampling positions. For each LAST position (Column 1), the number of proteins identified by DDA (Column 2) or HDMS^E (Column 3), total number of proteins (Column 4, excluding duplicate protein identification), proteins identified by DDA only (Column 6) or HDMS^E only (column 7) are provided.

LAST Sample ID	DDA	HDMS ^E	Total	_	Common to Both	DDA Only	HDMS ^E Only
Q1S1	341	814	847		308	33	506
Q1S2	322	1020	1030	_	312	10	708
Q1S3	393	1674	1680	_	387	6	1287
Q2S1	115	297	306	_	106	9	191
Q2S2	208	835	844	_	199	9	636
Q2S3	379	1723	1738	_	364	15	1359
Q3S1	133	751	755	_	129	4	622
Q3S2	326	1322	1341	_	307	19	1015
Q3S3	319	1139	1173	_	285	34	854
Q4S1	336	1369	1388	_	317	19	1052
Q4S2	365	1575	1589	_	351	14	1224
Q4S3	386	1204	1252	_	338	48	866

Considering 3478 proteins that were identified from the 12 laser ablation sampling positions, about 6% of the proteins were found in all 12 sampling positions (Figure S-3). Similarly, we expected that unique proteins would be identified from each sampling position

because different x-, y-, and z-coordinates were extracted from the brain. About 33% of proteins identified from laser ablated samples were found in only 1 of 12 positions. A spreadsheet document is also included with the Supporting Information (file name: Protein

Localization and Identification Frequency) that provides details on the spatial localization of each protein identified from LAST samples.

In DDA, precursor ions are selected for m/z-isolation and subsequent MS/MS based on their MS signal intensities. Precursorproduct ion correlation is straightforward because product ions are detected from m/z-isolated precursor ions. Although DDA does not explicitly use LC retention times for precursor-product ion correlation, shorter LC separation times can shift elution profiles of lower abundance peptides to highly congested regions where their selection for MS/MS may be limited by the instrument duty cycle (Supporting Figure S-4). Precursor-product ion correlation with HDMS^E requires a distinct "three-dimensional address" such as LC retention time, IM drift time, and m/z value for each precursor [54]. At shorter LC separation times, there are fewer unique retention times because there are fewer LC data points. Moreover, peak congestion at shorter LC separation times can result in more coelution. To evaluate the effect of separation speed on protein identification, we acquired UPLC-DDA and UPLC-HDMS^E data at LC separation times of 15, 30, 60, 90, 120, and 150 min. For these experiments, a whole brain tissue section was freshly prepared as a \sim 184 ng μ L⁻¹ tryptic digest.).

Fig. 3 shows the number of peptides (Fig. 3a) and proteins (Fig. 3b) identified by DDA and HDMS^E approaches at six different UPLC separation times ranging from 15 min to 150 min. As expected, shorter separation times resulted in (i) greater UPLC peak congestion (Supporting Figure S-5) and (ii) fewer peptides and proteins identified by both DDA (open white bars) and HDMS^E (solid black bars) analyses. Switching from the longest (150 min) to the shortest (15 min) measured UPLC separation times yielded fewer peptides (by 80%) and proteins (by 77%) identified *via* DDA; HDMS^E yielded two-thirds fewer identifications for both peptides and proteins. Moreover, HDMS^E outperformed DDA at all measured UPLC separation times (Fig. 3). For example, HDMS^E identified twice as many peptides and about 10% more proteins from the 15 min separation than DDA from the 150 min separation. Hence, HDMS^E was less sensitive to UPLC congestion than DDA.

4. Discussion

Here, we present the first application of IM enhanced DIA (HDMS^E) for high-throughput MS-based proteomics analyses of biological tissue extracts obtained via LAST. Results from analyses of rat brain tissue samples show that the HDMS^E approach identified more peptides and proteins than DDA. We also report the first comparison of DDA and HDMS^E as a function of UPLC separation time. On average for the twelve LAST samples, $94 \pm 2\%$ of the proteins identified by DDA were also identified by HDMS^E. Additionally, proteins were identified more confidently with HDMS^E than

DDA. Specifically, the average number of peptides detected per protein identified (from the twelve LAST samples) was 10.4 ± 1.4 for HDMS^E and 4.5 ± 0.7 for DDA.

The same precursor ions were present in corresponding DDA and HDMS^E datasets (Fig. 2); however, 73 ± 4% of the total proteins identified from each sampling position were not found by DDA. In DDA, current duty cycle limitations may not allow precursor ion selection for subsequent MS/MS, even if precursor ion signal intensities are above the user-defined threshold for ion selection (*i.e.*, >150 counts s⁻¹ in this study). Complementary HDMS^E data can reveal locations of these congested UPLC regions (*i.e.*, regions corresponding to elution of peptides not selected for MS/MS in DDA). For instance, as shown in Supporting Figure S-4, we were able to use complementary HDMS^E data to identify four low abundance peptides (in DDA data that were not selected for MS/MS) with UPLC retention times between 19.9 and 20.8 min.

Although UPLC-IM-MS data congestion precludes peptide identification in HDMS^E and adversely impacts protein identification, enhancing peak capacity in any of the three dimensions (i.e., UPLC, MS, or IM) could improve our ability to correlate product ions with their corresponding precursor ions. For instance, LC congestion can be addressed by using longer UPLC separations; however, the speed and sensitivity reduction associated with longer LC runs limit the utility of this approach for high-throughput applications. Moreover, higher mass resolving power and mass measurement accuracy can also enhance identification of LC co-eluting isobaric peptide ions in the m/z dimension. However, LC co-eluting isomers with the same chemical composition cannot be differentiated by increasing the peak capacity in the m/z dimension. Alternatively. higher IM resolving power can expand "data volume" such that LC co-eluting analytes with indistinguishable m/z values can be assigned unique three-dimensional addresses. Conventional approaches to increase IM resolving power include hardware modification, drift gas selection, and/or post acquisition data processing strategies. The latter is an attractive approach for improving IM resolving power because it requires no instrument modifications. Also, it can be applied to any post-IM tandem MS dataset. For instance, results in Table 1 for rat brain proteins missed by HDMS^E (identified by DDA only, column 4) suggest that higher IM peak capacity can increase the total number of identified proteins by 1%-3%. HDMS^E is unable to identify this small percentage of proteins primarily because of the three-dimensional data convolution of peptides used for protein identification. Hence, use of IM-MS deconvolution algorithms, such as automated ion mobility deconvolution (AIMD) [64], could enhance IM peak capacity and improve precursor-product ion correlation by allowing extraction of unique IM profiles, MS, and MS/MS spectra of species that are "hidden" in convoluted IM-MS datasets.

In addition to providing a more comprehensive overview of the

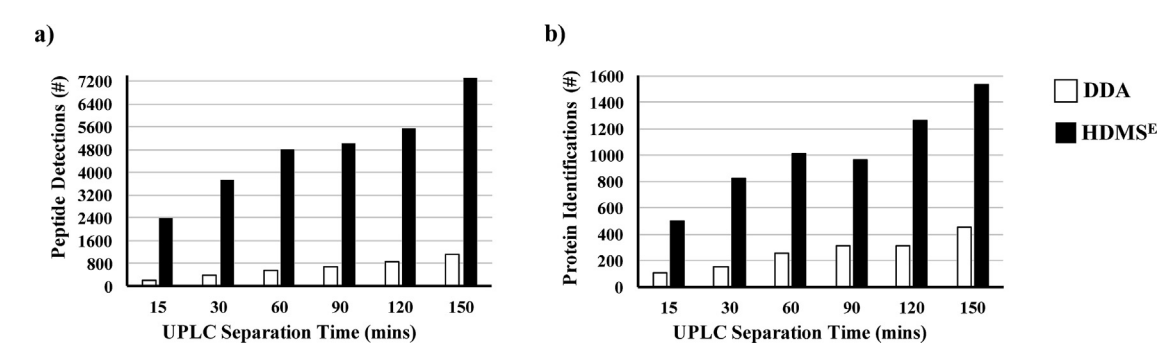


Fig. 3. Representation of the number of (a) peptides and (b) proteins identified by DDA (empty white bars) and HDMS^E (solid black bars) as a function of separation time. Separation times of 15, 30, 60, 120, and 150 min were used.

proteome in each laser ablated sampling quadrant, HDMS^E facilitated detection of proteins relevant to a broad range of disease related pathways that were not found by DDA analyses. As an example, we merged the "HDMS^E only" proteins (viz., Table 1) that were identified from Q1S1, Q1S2, and Q1S3, and then mapped them to the KEGG pathways database [65,66]. Table S-1 shows the proteins matching the pathways for cancer (Table S-1a, KEGG pathway: rno05200), Alzheimer's disease (Table S-1b, KEGG pathway: rno05010), and Parkinson's disease (Table S-1c, KEGG pathway: rno05012). In total, 63, 44, and 24 proteins, respectively, were successfully mapped to these pathways. The use of LAST and HDMS^E made it possible to identify proteins such as the ETS-1 transcription factor, which was linked to the invasion mechanism of malignant melanoma [67,68], and the Pim-1 serine/threonine kinase, which is part of the PIM family and has been linked to tumor growth [69,70]. Protein families such as the reticulon family (of which we detected the members 3 and 4) have been shown to provide insights in Alzheimer's disease related endoplasmic reticulum structural issues [71], and Parkinsonism associated deglycase has been long associated with onset and progression of Parkinson's disease [72].

5. Conclusions

Over four thousand proteins were identified by combined use of DDA and HDMS^E from high-throughput bottom-up proteomics analyses of rat brain tryptic digests from laser ablated and whole tissue samples (full list in Supporting Information Table S-2). Compared to collecting data in series with DDA, collecting ion fragmentation data in parallel as implemented in HDMS^E analysis resulted in identification of about seven times more peptides and about four times more proteins. Although more peptides and proteins are identified using HDMS^E, inherent differences between the serial and parallel data collection strategies render DDA and HDMS^E complementary strategies. For example, the combined use of both techniques increased the numbers of proteins identified by about 1%–3% for all measured samples. Analysis of a whole tissue digest sample as a function of UPLC separation time (i.e., comparing 150 and 15 min separations) demonstrated that chromatographic overlap reduced the number of proteins identified by about 80% for DDA and 67% for HDMS^E. At all measured times for UPLC separation, HDMS^E identified more peptides and proteins than DDA. The ability to pinpoint UPLC regions that are congested can provide crucial information to judiciously improve UPLC separations in a manner that would enhance MS/MS selection by DDA or decrease three-dimensional data convolutions in HDMS^E.

Acknowledgements

This material is based upon work supported by the National Science Foundation under Grant No. IDBR-1455668 and Grant No. CHE-1709526.

Appendix A. Supplementary data

Supplementary data related to this article can be found at https://doi.org/10.1016/j.aca.2018.06.066.

References

- [1] L.C. Gillet, A. Leitner, R. Aebersold, Mass spectrometry applied to bottom-up proteomics: entering the high-throughput era for hypothesis testing, Annu. Rev. Anal. Chem. 9 (2016) 449–472.
- [2] S.-E. Ong, M. Mann, Mass spectrometry—based proteomics turns quantitative, Nat. Chem. Biol. 1 (2005) 252–262.
- [3] J.L. Norris, R.M. Caprioli, Analysis of tissue specimens by matrix-assisted laser

- desorption/ionization imaging mass spectrometry in biological and clinical research, Chem. Rev. 113 (2013) 2309–2342.
- [4] M.M. Gessel, J.L. Norris, R.M. Caprioli, MALDI imaging mass spectrometry: spatial molecular analysis to enable a new age of discovery, J. Proteomics 107 (2014) 71–82.
- [5] C.B. Lietz, E. Gemperline, L. Li, Qualitative and quantitative mass spectrometry imaging of drugs and metabolites, Adv. Drug Deliv. Rev. 65 (2013) 1074–1085.
- [6] J. Franck, J. Quanico, M. Wisztorski, R. Day, M. Salzet, I. Fournier, Quantification-based mass spectrometry imaging of proteins by parafilm assisted microdissection. Anal. Chem. 85 (2013) 8127—8134.
- [7] P. Loziuk, F. Meier, C. Johnson, H.T. Ghashghaei, D.C. Muddiman, TransOmic analysis of forebrain sections in Sp2 conditional knockout embryonic mice using IR-MALDESI imaging of lipids and LC-MS/MS label-free proteomics, Anal. Bioanal. Chem. 408 (2016) 3453–3474.
- [8] S.K. Maier, H. Hahne, A.M. Gholami, B. Balluff, S. Meding, C. Schoene, A.K. Walch, B. Kuster, Comprehensive identification of proteins from MALDI imaging, Mol. Cell. Proteomics 12 (2013) 2901–2910.
- [9] J. Quanico, J. Franck, C. Dauly, K. Strupat, J. Dupuy, R. Day, M. Salzet, I. Fournier, M. Wisztorski, Development of liquid microjunction extraction strategy for improving protein identification from tissue sections, J. Proteomics 79 (2013) 200–218.
- [10] J. Sarsby, N.J. Martin, P.F. Lalor, J. Bunch, H.J. Cooper, Top-down and bottom-up identification of proteins by liquid extraction surface analysis mass spectrometry of healthy and diseased human liver tissue, J. Am. Soc. Mass Spectrom. 25 (2014) 1953–1961.
- [11] M. Assadi, J. Lamerz, T. Jarutat, A. Farfsing, H. Paul, B. Gierke, E. Breitinger, M.F. Templin, L. Essioux, S. Arbogast, Multiple protein analysis of formalinfixed and paraffin-embedded tissue samples with reverse phase protein arrays, Mol. Cell. Proteomics 12 (2013) 2615–2622.
- [12] M.S. Scicchitano, D.A. Dalmas, R.W. Boyce, H.C. Thomas, K.S. Frazier, Protein extraction of formalin-fixed, paraffin-embedded tissue enables robust proteomic profiles by mass spectrometry, J. Histochem. Cytochem. 57 (2009) 849–860.
- [13] W. Zhang, S. Sakashita, P. Taylor, M.S. Tsao, M.F. Moran, Comprehensive proteome analysis of fresh frozen and optimal cutting temperature (OCT) embedded primary non-small cell lung carcinoma by LC–MS/MS, Methods 81 (2015) 50–55.
- [14] J.M. Spraggins, D.G. Rizzo, J.L. Moore, K.L. Rose, N.D. Hammer, E.P. Skaar, R.M. Caprioli, MALDI FTICR IMS of intact proteins: using mass accuracy to link protein images with proteomics data, J. Am. Soc. Mass Spectrom. 26 (2015) 974–985
- [15] J. Quanico, J. Franck, J.P. Gimeno, R. Sabbagh, M. Salzet, R. Day, I. Fournier, Parafilm-assisted microdissection: a sampling method for mass spectrometrybased identification of differentially expressed prostate cancer protein biomarkers, Chem. Commun. 51 (2015) 4564–4567.
- [16] J. Quanico, J. Franck, M. Wisztorski, M. Salzet, I. Fournier, Integrated mass spectrometry imaging and omics workflows on the same tissue section using grid-aided, parafilm-assisted microdissection, BBA-Gen. Subjects 1871 (2017) 1702—1714.
- [17] N. Simone, R. Bonner, J. Gillespie, M. Emmert-Buck, L. Liotta, Laser-capture microdissection: opening the microscopic frontier to molecular analysis, Trends Genet. 14 (1998) 272–276.
- [18] L. Cheng, S. Zhang, D. Davidson, M. Kuhar, M. Wang, S. Williamson, D. Zhang, G. MacLennan, Laser capture microdissection in molecular diagnostics, in: L. Cheng, D.Y. Zhang, J.N. Eble (Eds.), Molecular Genetic Pathology, Springer, New York, 2012, pp. 465–482.
- [19] L.G. Legres, A. Janin, C. Masselon, P. Bertheau, Beyond laser microdissection technology: follow the yellow brick road for cancer research, Am. J. Canc. Res. 4 (2014) 1–28.
- [20] D.E. Palmer-Toy, D.A. Sarracino, D. Sgroi, R. LeVangie, P.E. Leopold, Direct acquisition of matrix-assisted laser desorption/ionization time-of-flight mass spectra from laser capture microdissected tissues, Clin. Chem. 46 (2000) 1513—1516
- [21] S.H. Bhattacharya, A. Gal, K.K. Murray, Laser capture microdissection MALDI for direct analysis of archival tissue, J. Proteome Res. 2 (2003) 95–98.
- [22] B. Xu, R.M. Caprioli, M. Sanders, R. Jensen, Direct analysis of laser capture microdissected cells by MALDI mass spectrometry, J. Am. Soc. Mass Spectrom. 13 (2002) 1292–1297.
- [23] J.S. Becker, S. Niehren, A. Matusch, B. Wu, H.F. Hsieh, U. Kumtabtim, M. Hamester, A. Plaschke-Schlütter, D. Salber, Scaling down the bioimaging of metals by laser microdissection inductively coupled plasma mass spectrometry (LMD-ICP-MS), Int. J. Mass Spectrom. 294 (2010) 1–6.
- [24] S.J. Geromanos, J.P. Vissers, J.C. Silva, C.A. Dorschel, G.Z. Li, M.V. Gorenstein, R.H. Bateman, J.I. Langridge, The detection, correlation, and comparison of peptide precursor and product ions from data independent LC-MS with data dependent LC-MS/MS, Proteomics 9 (2009) 1683–1695.
- [25] J. He, J. Zhu, Y. Liu, J. Wu, S. Nie, J.A. Heth, K.M. Muraszko, X. Fan, D.M. Lubman, Immunohistochemical staining, laser capture microdissection, and filter-aided sample preparation-assisted proteomic analysis of target cell populations within tissue samples, Electrophoresis 34 (2013) 1627—1636.
- [26] J. Zhu, S. Nie, J. Wu, D.M. Lubman, Target proteomic profiling of frozen pancreatic CD24+ adenocarcinoma tissues by immuno-laser capture micro-dissection and nano-LC-MS/MS, J. Proteomics Res. 12 (2013) 2791–2804.
- [27] S. Hebbar, W.D. Schulz, U. Sauer, D. Schwudke, Laser capture microdissection

- coupled with on-column extraction LC-MSⁿ enables lipidomics of fluorescently labeled *Drosophila* neurons, Anal. Chem. 86 (2014) 5345–5352.
- [28] S. Sethi, J.A. Vrana, J.D. Theis, N. Leung, A. Sethi, S.H. Nasr, F.C. Fervenza, L.D. Cornell, M.E. Fidler, A. Dogan, Laser microdissection and mass spectrometry-based proteomics aids the diagnosis and typing of renal amyloidosis, Kidney Int. 82 (2012) 226–234.
- [29] M.Z. Huang, S.S. Jhang, C.N. Cheng, S.C. Cheng, J. Shiea, Effects of matrix, electrospray solution, and laser light on the desorption and ionization mechanisms in electrospray-assisted laser desorption ionization mass spectrometry, Analyst 135 (2010) 759–766.
- [30] M. Lorenz, O.S. Ovchinnikova, G.J. Van Berkel, Fully automated laser ablation liquid capture surface analysis using nanoelectrospray ionization mass spectrometry, Rapid Commun. Mass Spectrom. 28 (2014) 1312–1320.
- [31] O.S. Ovchinnikova, V. Kertesz, G.J. Van Berkel, Combining laser ablation/liquid phase collection surface sampling and high-performance liquid Chromatography—Electrospray ionization-mass spectrometry, Anal. Chem. 83 (2011) 1874–1878.
- [32] S.-G. Park, K.K. Murray, Infrared laser ablation sample transfer for MALDI and electrospray, J. Am. Soc. Mass Spectrom. 22 (2011) 1352–1362.
- [33] S.-G. Park, K.K. Murray, Infrared laser ablation sample transfer for on-line liquid chromatography electrospray ionization mass spectrometry, J. Mass Spectrom. 47 (2012) 1322–1326.
- [34] S.-G. Park, K.K. Murray, Ambient laser ablation sampling for capillary electrophoresis mass spectrometry, Rapid Commun. Mass Spectrom. 27 (2013) 1673–1680.
- [35] F. Donnarumma, K.K. Murray, Laser ablation sample transfer for localized LC-MS/MS proteomic analysis of tissue, J. Mass Spectrom. 51 (2016) 261–268.
- [36] B. Domon, R. Aebersold, Review mass spectrometry and protein analysis, Science 312 (2006) 212–217.
- [37] M. Bern, G. Finney, M.R. Hoopmann, G. Merrihew, M.J. Toth, M.J. MacCoss, Deconvolution of mixture spectra from ion-trap data-independent-acquisition tandem mass spectrometry, Anal. Chem. 82 (2009) 833–841.
- [38] P.C. Carvalho, X. Han, T. Xu, D. Cociorva, M.d.G. Carvalho, V.C. Barbosa, J.R. Yates III, XDIA: improving on the label-free data-independent analysis, Bioinformatics 26 (2010) 847–848.
- [39] T. Geiger, J. Cox, M. Mann, Proteomics on an Orbitrap benchtop mass spectrometer using all-ion fragmentation, Mol. Cell. Proteomics 9 (2010) 2252–2261.
- [40] L.C. Gillet, P. Navarro, S. Tate, H. Rost, N. Selevsek, L. Reiter, R. Bonner, R. Aebersold, Targeted data extraction of the MS/MS spectra generated by data-independent acquisition: a new concept for consistent and accurate proteome analysis, Mol. Cell. Proteomics 11 (2012). 0111.016717—0016111.016717.
- [41] A. Panchaud, S. Jung, S.A. Shaffer, J.D. Aitchison, D.R. Goodlett, Faster, quantitative, and accurate precursor acquisition independent from ion count, Anal. Chem. 83 (2011) 2250–2257.
- [42] A. Panchaud, A. Scherl, S.A. Shaffer, P.D. Von Haller, H.D. Kulasekara, S.I. Miller, D.R. Goodlett, Precursor acquisition independent from ion count: how to dive deeper into the proteomics ocean, Anal. Chem. 81 (2009) 6481–6488.
- [43] R.S. Plumb, K.A. Johnson, P. Rainville, B.W. Smith, I.D. Wilson, J.M. Castro-Perez, J.K. Nicholson, UPLC/MSE; a new approach for generating molecular fragment information for biomarker structure elucidation, Rapid Commun. Mass Spectrom. 20 (2006) 1989–1994.
- [44] S. Purvine, E.C. Yi, D.R. Goodlett, Shotgun collision-induced dissociation of peptides using a time of flight mass analyzer, Proteomics 3 (2003) 847–850.
- [45] J.D. Venable, M.-Q. Dong, J. Wohlschlegel, A. Dillin, J.R. Yates, Automated approach for quantitative analysis of complex peptide mixtures from tandem mass spectra, Nat. Methods 1 (2004) 39–45.
- [46] P. Fellgett, On the ultimate sensitivity and practical performance of radiation detectors, J. Opt. Soc. Am. 39 (1949) 970–976.
- [47] D.E. Clemmer, R.R. Hudgins, M.F. Jarrold, Naked protein conformations: cy-tochrome c in the gas phase, J. Am. Chem. Soc. 117 (1995) 10141–10142.
- [48] K. Giles, S.D. Pringle, K.R. Worthington, D. Little, J.L. Wildgoose, R.H. Bateman, Applications of a travelling wave-based radio-frequency-only stacked ring ion guide, Rapid Commun. Mass Spectrom. 18 (2004) 2401–2414.
- [49] S.D. Pringle, K. Giles, J.L. Wildgoose, J.P. Williams, S.E. Slade, K. Thalassinos,

- R.H. Bateman, M.T. Bowers, J.H. Scrivens, An investigation of the mobility separation of some peptide and protein ions using a new hybrid quadrupole/travelling wave IMS/oa-ToF instrument, Int. J. Mass Spectrom. 261 (2007) 1–12
- [50] T. Wyttenbach, G. von Helden, M.T. Bowers, Gas-phase conformation of biological Molecules: bradykinin, J. Am. Chem. Soc. 118 (1996) 8355–8364.
- [51] J.C. Silva, M.V. Gorenstein, G.-Z. Li, J.P. Vissers, S.J. Geromanos, Absolute quantification of proteins by LC-MS^E a virtue of parallel MS acquisition, Mol. Cell. Proteomics 5 (2006) 144–156.
- [52] N.J. Bond, P.V. Shliaha, K.S. Lilley, L. Gatto, Improving qualitative and quantitative performance for MSE-based label-free proteomics, J. Proteome Res. 12 (2013) 2340–2353.
- [53] U. Distler, J. Kuharev, P. Navarro, Y. Levin, H. Schild, S. Tenzer, Drift timespecific collision energies enable deep-coverage data-independent acquisition proteomics, Nat. Methods 11 (2014) 167–170.
- [54] S.J. Geromanos, C. Hughes, S. Ciavarini, J.P. Vissers, J.I. Langridge, Using ion purity scores for enhancing quantitative accuracy and precision in complex proteomics samples, Anal. Bioanal. Chem. 404 (2012) 1127–1139.
- [55] P.V. Shliaha, N.J. Bond, L. Gatto, K.S. Lilley, Effects of traveling wave ion mobility separation on data independent acquisition in proteomics studies, I. Proteome Res. 12 (2013) 2323–2339.
- [56] U. Consortium, UniProt: a hub for protein information, Nucleic Acids Res. 43 (2015) D204–D212.
- [57] C. Chen, Z. Li, H. Huang, B.E. Suzek, C.H. Wu, U. Consortium, A fast peptide match service for UniProt knowledgebase, Bioinformatics 29 (2013) 2808–2809.
- [58] B. Paizs, S. Suhai, Fragmentation pathways of protonated peptides, Mass Spectrom. Rev. 24 (2005) 508–548.
- [59] M. Vandenbogaert, S. Li-Thiao-Té, H.M. Kaltenbach, R. Zhang, T. Aittokallio, B. Schwikowski, Alignment of LC-MS images, with applications to biomarker discovery and protein identification, Proteomics 8 (2008) 650–672.
- [60] J.D. Venable, J.R. Yates, Impact of ion trap tandem mass spectra variability on the identification of peptides, Anal. Chem. 76 (2004) 2928–2937.
- [61] U.D. Neue, C.H. Phoebe, K. Tran, Y.-F. Cheng, Z. Lu, Dependence of reversed-phase retention of ionizable analytes on pH, concentration of organic solvent and silanol activity, J. Chromatogr. Abstr. 925 (2001) 49–67.
- [62] T. Wyttenbach, P.R. Kemper, M.T. Bowers, Design of a new electrospray ion mobility mass spectrometer, Int. J. Mass Spectrom. 212 (2001) 13–23.
- [63] E.A. Mason, E.W. McDaniel, Transport Properties of Ions in Gases, NASA STI/ Recon Technical Report a 89, 1988.
- [64] M. Brantley, B. Zekavat, B. Harper, R. Mason, T. Solouki, Automated deconvolution of overlapped ion mobility profiles, J. Am. Soc. Mass Spectrom. 25 (2014) 1810–1819.
- [65] KEGG, Kyoto encyclopedia of genes and genomes. https://www.kegg.jp/. (Accessed 19 June 2018).
- [66] M. Kanehisa, M. Furumichi, M. Tanabe, Y. Sato, K. Morishima, KEGG: new perspectives on genomes, pathways, diseases and drugs, Nucleic Acids Res. 45 (2016) D353–D361.
- [67] Y. Li, H. Luo, T. Liu, E. Zacksenhaus, Y. Ben-David, The ets transcription factor Fli-1 in development, cancer and disease, Oncogene 34 (2015) 2022.
- [68] T. Rothhammer, J. Hahne, A. Florin, I. Poser, F. Soncin, N. Wernert, A.-K. Bosserhoff, The Ets-1 transcription factor is involved in the development and invasion of malignant melanoma, Cell. Mol. Life Sci. 61 (2004) 118–128.
- [69] R.F. Fan, Y. Lu, Z.G. Fang, X.Y. Guo, Y.X. Chen, Y.C. Xu, Y.M. Lei, K.F. Liu, D.J. Lin, L.L. Liu, PIM-1 kinase inhibitor SMI-4a exerts antitumor effects in chronic myeloid leukemia cells by enhancing the activity of glycogen synthase kinase 3β, Mol. Med. Rep. 16 (2017) 4603–4612.
- [70] M. Narlik-Grassow, C. Blanco-Aparicio, A. Carnero, The PIM family of serine/ threonine kinases in cancer, Med. Res. Rev. 34 (2014) 136–159.
- [71] M.G. Sharoar, Q. Shi, Y. Ge, W. He, X. Hu, G. Perry, X. Zhu, R. Yan, Dysfunctional tubular endoplasmic reticulum constitutes a pathological feature of Alzheimer's disease, Mol. Psychiatr. 21 (2016) 1263.
- [72] R. Bandopadhyay, A.E. Kingsbury, M.R. Cookson, A.R. Reid, I.M. Evans, A.D. Hope, A.M. Pittman, T. Lashley, R. Canet-Aviles, D.W. Miller, The expression of DJ-1 (PARK7) in normal human CNS and idiopathic Parkinson's disease, Brain 127 (2004) 420–430.